

Multi-Kernel Polar Codes: Concept and Design Principles

Valerio Bioglio, Frédéric Gabry, Ingmar Land, Jean-Claude Belfiore
Mathematical and Algorithmic Sciences Lab

France Research Center, Huawei Technologies France SASU

Email: {valerio.bioglio,frederic.gabry,ingmar.land,jean.claude.belfiore}@huawei.com

Abstract—In this paper, we propose a new polar code construction by employing kernels of different sizes in the Kronecker product of the transformation matrix, thus generalizing the original construction by Arikan. The proposed multi-kernel polar code allows for more flexibility in terms of the code length, moreover allowing for various new design principles. We describe in detail encoding as well as successive cancellation (SC) decoding and SC list (SCL) decoding, and we provide a novel design method for the frozen set that allows to optimise the performance under list decoding, as opposed to original reliability-based code design. Finally, we numerically demonstrate the advantage of multi-kernel polar codes under the new design principles compared to punctured and shortened polar codes.

I. INTRODUCTION

Polar codes are a family of error-correcting codes recently introduced by Arikan in [1] as the first codes able to provably achieve channel capacity for a large number of channels. The construction of a polar code of length $N = 2^n$ is based on the recursive concatenation of the binary matrix $T_2 = \begin{pmatrix} 1 & 0 \\ 1 & 1 \end{pmatrix}$, referred to as the kernel of the transformation. This operation results in a transformation matrix $T_N = T_2^{\otimes n}$, given by the n -fold Kronecker power of the kernel matrix T_2 , converting the physical channel into N virtual synthetic channels characterized by either very high or very low reliability. This channel polarization effect leads to a portion of fully reliable channels that tends to the channel capacity for symmetric binary-input memoryless channels, when the code length tends to infinity. In the asymptotic case, successive cancellation (SC) decoding is sufficient to achieve the channel capacity [1]. In the finite-length regime, successive cancellation list (SCL) decoding [2] leads to performance competitive with many other classes of channel codes, like LDPC codes, particularly when an outer CRC code or generalizations thereof are applied [3]. Due to their excellent performance, polar codes were recently adopted as moderate-length codes for 5G [4].

As conjectured in [1], the polarization phenomenon obtained by the Kronecker powers of T_2 can be extended to other kernels. In [5], authors show necessary and sufficient conditions for kernels to polarize, allowing researchers to propose larger binary kernels as bases of novel polar codes [6]. Non-binary kernels have been proposed to improve the asymptotic error probability [7], [8], while mixing binary and non-binary kernels showed additional improvement over homogeneous kernels constructions [9]. As a result, current constructions restrict the length of polar codes to be in the form $N = l^n$.

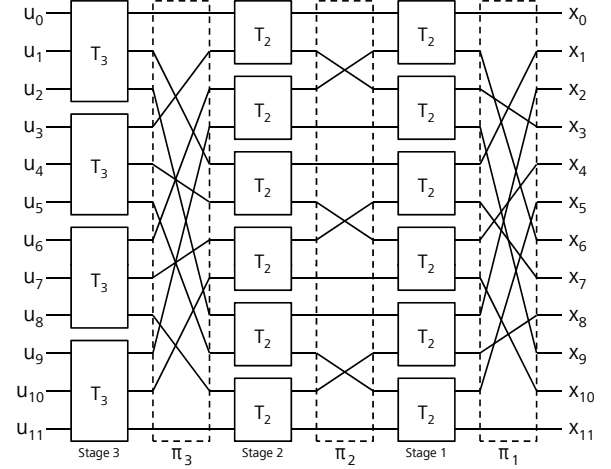


Fig. 1: Tanner graph of the multi-kernel polar code of length $N = 12$ for the transformation matrix $T_{12} = T_2 \otimes T_2 \otimes T_3$.

This code length constraint can be a huge limitation to practical use of polar codes, since only few block lengths can be expressed as a power of an integer. Punctured [10] and shortened [11] polar codes have been proposed to increase the number of achievable block lengths. Even if these techniques offer a practical way to construct codes of arbitrary lengths, they show many disadvantages. In fact, punctured and shortened codes are decoded by means of their mother polar codes, increasing the decoding latency with respect to the actual code length. Moreover, the location of dummy bits, altering the polarization of the codes, has to be carefully chosen to avoid catastrophic error-rate performance [12]. Finally, the lack of structure between the frozen sets and the puncturing or shortening patterns complicates the code design [13].

In this paper, we present multi-kernel polar codes, which generalize polar codes by mixing kernels of different sizes over the same binary alphabet. These codes were theorized in [14], where their polarization rate is calculated algebraically, and explicitly constructed in [15]; they conceptually permit to construct polar codes of any block length while keeping the polarization effect [16]. The encoding follows the general structure of polar codes, and the decoding can be performed by successive cancellation as well. Building on our previous contributions in [15] and [17], in this paper we present a thorough description and analysis of construction of multi-kernel polar codes, discussing the issues related to the choice of

component kernels. Finally, similarly to [18] we combine the aforementioned designs into a novel hybrid design exhibiting good error correction performance at moderate length.

This paper is organized as follows. In Section II, we present the general construction, including the encoding and decoding, of multi-kernel polar codes. In Section III we provide recommendations for the selection of kernels to be used in the multi-kernel construction. In Section IV we describe explicitly the different designs for multi-kernel polar codes, namely by reliability, by minimum distance, and by a hybrid criterion. In Section V we discuss the performance of the proposed codes, and Section VI concludes this paper.

II. CODE AND DECODER

In this section, we introduce the structure, encoding and decoding of multi-kernel polar codes. As an example, the Tanner graph of a code of length $N = 12$ is depicted in Fig. 1, comprising two kernels of size 2 and one kernel of size 3.

A. Code Structure and Encoding

Multi-kernel polar codes are a generalization of Arikan's polar codes obtained by using binary kernels of different sizes in the construction of the transformation matrix of the code. An (N, K) multi-kernel polar code of length N and dimension K is defined by a $N \times N$ transformation matrix

$$T_N = T_{p_1} \otimes T_{p_2} \otimes \dots \otimes T_{p_s}, \quad (1)$$

with $N = p_1 \cdot p_2 \cdot \dots \cdot p_s$, and a frozen set $\mathcal{F} \subset [N]$, where $[N] = \{0, 1, 2, \dots, N-1\}$, such that $|\mathcal{F}| = N - K$. The information set is defined as $\mathcal{I} = \mathcal{F}^C$. Building blocks of the code are the $p_i \times p_i$ matrices T_{p_i} with binary entries, which define kernels of dimension p_i [19]. A list of binary polarizing kernels with maximum exponents, i.e. maximum polarization, can be found in [7]. However, other kernels may be advantageous for the design of multi-kernel polar codes, as described in Sec. III. The frozen set collects the indices of the input vector to be frozen: its design will be discussed in Section IV. Codewords $x \in \mathbb{F}_2^N$ are generated from the input vector $u \in \mathbb{F}_2^N$ by $x = u \cdot T_N$, where $u_j = 0$ for $j \in \mathcal{F}$ and the remaining K entries of u_i for $i \in \mathcal{I}$ store the information to be transmitted. Note that outer CRCs or similar parity checks may be inserted as for original polar codes. In the following, we will refer to polar codes when the transformation matrix is generated using a single kernel according to the original formulation by Arikan, while we will refer to multi-kernel polar codes if more than one binary kernel is used in the transformation matrix generation.

The order of the kernels in (1) is important for the design of the code, as this operation is not commutative. Changing the order of kernels in T_N is equivalent to permuting its rows and columns, since for any Kronecker product there exist two permutation matrices P, Q such that $A \otimes B = P \cdot (B \otimes A) \cdot Q$ [20]. In practice, changing the order of the kernels leads to a transformation matrix in which rows and columns are permuted as compared to the original transformation matrix. Every frozen set imposed on the original matrix can hence be mapped in a frozen set of the permuted matrix: all the

kernel orders lead to equivalent codes. However, this order may have an effect on the polarization of the virtual channels as discussed in Section IV-A.

B. Tanner Graph

The structure of multi-kernel polar codes can be illustrated by the Tanner graph as depicted in Figure 1. This graph describes the transformation matrix T_N of the code, and consists of various $p_i \times p_i$ boxes, each corresponding to a kernel T_{p_i} which defines the relation between the input vector and the output vector. A $p_i \times p_i$ box has p_i inputs and outputs. A stage of the graph corresponds to a factor in the Kronecker product of the transformation matrix, and is depicted by N/p_i boxes vertically distributed, for a total of s stages, counted from the codeword x (right) to the input vector u (left).

The connections between stages are implicitly defined by the Kronecker product. Stage i has N/p_i boxes, each one representing a kernel T_{p_i} , that are connected to the N/p_{i-1} boxes of stage $i-1$ through an edge permutation π_i . These permutations operate in blocks, where two boxes in different blocks are not connected. Denoting $N_i = \prod_{j=1}^{i-1} p_j$ the partial product of the kernel sizes up to stage i , with $N_1 = 1$, we can divide the boxes forming stages i and $i-1$ in N/N_{i+1} blocks. Inside a block, boxes of stages $i-1$ are further divided into N_i sub-blocks, so that the j -th box of stage i is connected to the j -th output of each sub-block of stage $i-1$. This canonical permutation ρ_i , depicted in Equation (2), will be used as a basis to create the general permutations between stages. In fact, given the canonical permutation ρ_i , the permutation π_i is given by $\pi_i = (\rho_i | \rho_i + N_{i+1} | \rho_i + 2N_{i+1} | \dots | \rho_i + (N/N_{i+1} - 1)N_{i+1})$ for $i = 2, \dots, s$. Note that for the last stage, we have $\pi_s = \rho_s$. First permutation π_1 , acting like the bit-reversal permutation for polar codes, is an exception obtained inverting the product of the other permutations as $\pi_1 = (\pi_2 \cdot \dots \cdot \pi_s)^{-1}$.

C. Decoding

Decoding of multi-kernel polar codes is performed by successive cancellation (SC) [1] on the Tanner graph of the code. Similar to polar codes, enhanced SC-based decoding methods, like simplified SC (SSC) [21], SC list (SCL) [2] or SC stack decoding [22] may be employed. In SC, bits are decoded sequentially using the log-likelihood ratios (LLRs) of the received symbols along with the (estimated) previously decoded bits. If λ_i corresponds to the LLR of input bit u_i , an SC decoder sequentially evaluates

$$\lambda_i = f_i^N(l_0, l_1, \dots, l_{N-1}, \hat{u}_0, \hat{u}_1, \dots, \hat{u}_{i-1}) \quad (3)$$

for every i from 0 to $N-1$, where l_i corresponds to the LLR of the codebit x_i . In the following, we assume a BPSK transmission over an AWGN channel, referred to as the BI-AWGN, denoting with E_s the energy of the transmitted symbols and with N_0 the single-sided noise power density. With constellation points ± 1 , the SNR may be given in E_s/N_0 or in $E_b/N_0 = 1/R \cdot E_s/N_0$, where R denotes the code rate and $\sigma^2 = N_0/(2E_s)$ is the variance of the AWGN. With

$$\rho_i = \begin{pmatrix} 1 & 2 & \dots & N_i & N_i + 1 & N_i + 2 & \dots & (n_i - 1)N_i + 1 & \dots & N_{i+1} \\ 1 & p_i + 1 & \dots & (N_i - 1)p_i + 1 & 2 & p_i + 2 & \dots & p_i & \dots & N_{i+1} \end{pmatrix} \quad (2)$$

$y = [y_0, \dots, y_{N-1}]$ denoting the output of the BI-AWGN channel, the channel LLRs are computed as $l_i = 2y_i/\sigma^2$.

The recursive structure of the transformation matrix of multi-kernel polar codes, like polar codes, permits to drastically reduce the decoding complexity by performing the LLR computation on a kernel base. In fact, LLRs can be calculated in the kernel boxes and passed along the Tanner graph of the code to the other kernel boxes from the right to the left, with hard decisions on decoded bits flowing from left to right. These hard decisions, representing the estimates of the intermediate bits, are used by kernel boxes to calculate intermediate LLRs.

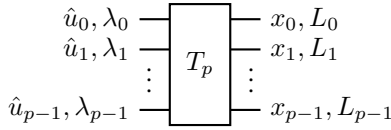


Fig. 2: A $p \times p$ box corresponding to kernel T_p .

The $p \times p$ box corresponding to a T_p kernel is depicted in Fig. 2, having $u = [u_0, u_1, \dots, u_{p-1}]$ as input vector and $x = [x_0, x_1, \dots, x_{p-1}]$ as output vector. Hard decisions on the output vector are calculated via multiplication with the kernel matrix, as $\hat{x} = \hat{u} \cdot T_p$. The LLR calculation is more complex; denoting by L_i the input LLRs and by λ_i the output LLRs (seen right to left), the SC equation (3) can be simplified as

$$\lambda_i = f_i^p(L_0, L_1, \dots, L_{p-1}, \hat{u}_0, \hat{u}_1, \dots, \hat{u}_{i-1}), \quad (4)$$

taking into account only LLRs and bit estimates belonging to the present box. The formulation of the LLR update functions f_i^p for specific kernels will be discussed in Sec. III.

III. KERNEL ANALYSIS

The polarization phenomenon, originally proved for matrix T_2 , has been extended to binary matrices in [5] and to arbitrary finite fields in [19], where sufficient and necessary conditions are provided for a square matrix to polarize. A polarizing matrix is called *kernel*, and can be used in the construction of polar codes. Multi-kernel polar codes are based on the generalized polarization effect obtained mixing kernels of different sizes [16]. Compared to polar codes, our construction permits to exploit the distance properties of the kernels to improve the error correction performance, in particular for small block lengths. Here we analyze the structure and the decoding complexity of large kernels, providing recommendations for the design of kernels for multi-kernel polar codes.

A. Minimum-Distance Spectrum

The speed of polarization of a kernel is evaluated via the polarization exponent [7], calculated through the partial distances of the kernel matrix. These partial distances are defined as the minimum weights of a sequence given by

the sum of a row and any linear combination of following rows. This notion is based on the nature of SC decoding, and is used to drive the kernel design. Under SCL decoding, however, polar codes show better performance than predicted by the polarization exponent. Moreover, the polarization effect is less important than distance properties for short codes, and kernels should be designed taking this aspect into account. We conjecture the notion of minimum-distance spectrum [17] to be more effective in these scenarios.

The *minimum-distance spectrum* S_{T_p} of a kernel T_p is defined as the mapping from dimension k , $k = 1, 2, \dots, p$, to the largest minimum distance achievable by any (p, k) sub-code of T_p , i.e. by any code having k rows of T_p as generator matrix. More formally, if $T_p^{(\mathcal{R})}$ is the matrix formed by the rows of T_p indexed by $\mathcal{R} \subset [p]$ and $d(A)$ is the minimum distance of the code generated by the rows of matrix A , then the minimum-distance spectrum of T_p is defined as

$$S_{T_p}(k) = \max_{|\mathcal{R}|=k} d\left(T_p^{(\mathcal{R})}\right), \quad (5)$$

for $k = 1, \dots, p$. Optimal row set $\mathcal{R}_p^k \subset [p]$ collects the indices of the k rows of T_p forming the generator matrix of the optimal $(p, k, S_{T_p}(k))$ code extracted from the kernel.

The minimum-distance spectrum can be seen as a generalization of partial distances. In fact, partial distances are obtained as the distances determined by selecting the rows bottom up. As a result, row sets are nested, every row set being a subset of all larger ones. The minimum-distance spectrum relaxes this constraint, allowing for non-nested information sets, and thus providing a new degree of freedom for the overall code design. While partial distances are conceived for characterizing SC decoding, the minimum-distance spectrum seems to be more effective in portraying SCL decoding.

B. Kernel Decoding

Formulation of decoding equations (4) for the LLR calculation under SC decoding is of capital importance during kernel design. With reference to Fig. 2, the (input) LLRs L_i derive from previous decoding steps or, if the kernel is in the first stage, are the LLRs of bits x_j , $L_j = L(x_j)$, calculated from the received symbols; the (output) LLRs λ_i represent the LLRs of bits u_i , $\lambda_i = L(u_i)$. They can be expressed using only input LLRs and hard decisions of the previously decoded bits u_0, \dots, u_{i-1} , as

$$\lambda_i = \ln \frac{\sum_{x \in X_0^{(i)}} \exp\left(\sum_{t=0}^{p-1} (1 - x_t) L_t\right)}{\sum_{x \in X_1^{(i)}} \exp\left(\sum_{t=0}^{p-1} (1 - x_t) L_t\right)}, \quad (6)$$

$X_a^{(i)} = \{v \cdot G : v = [u_0, \dots, u_{i-1}, a, v_{i+1}, \dots, v_{p-1}], v_j \in \mathbb{F}_2\}$, $a = 0, 1$, which corresponds to the marginalization over the unknown bits v_{i+1}, \dots, v_{p-1} [23]. Since $|X_a^{(i)}| = 2^{p-i}$, to compute this expression is in general exponential in the kernel

size p , even if it can be simplified by human inspection [24] or trellis-based decoding of block codes [25]. However, this formulation complicates the calculation of input-bit reliability, restricting the design of the code to Monte-Carlo methods.

In practice, analysis of the tree of recurrent relations of the graph induced by the kernel matrix may permit to discriminate among the different channel observations, rewriting expression (6) using only basic operations of the LLR algebra [26]; if bits x_1, \dots, x_j represent a repetition of bit x_0 and the corresponding LLRs L_i are based on independent observations, then

$$L(x_0|L_0, \dots, L_j) = L_0 + \dots + L_j. \quad (7)$$

On the other hand, if x_0, \dots, x_j are independent bits and the LLRs L_i are based on independent observations, then

$$L(x_0 \oplus \dots \oplus x_j) = L_0 \boxplus \dots \boxplus L_j \quad (8)$$

where the \boxplus operation is defined as

$$\sum \boxplus a_t \triangleq 2 \tanh^{-1} \left(\prod_{t=0}^j \tanh \frac{a_t}{2} \right) \approx \min_{0 \leq t \leq j} (|a_t|) \cdot \prod_{t=0}^j \operatorname{sgn} a_t.$$

If it is possible to formulate (6) with an expression involving only $+$ and \boxplus operations of the LLRs L_0, \dots, L_{p-1} , we say that the decoding equation is expressed in *reduced form*. In such a case, the complexity becomes linear in p , and the analysis of the kernel polarization can be simplified as explained in the next sections. Reducibility of general decoding equations being an open problem, we conjecture that (6) cannot be expressed in reduced form for all bit positions and all kernels; we suggest to approximate irreducible expressions with similar expressions in reduced form.

C. Kernel Examples

Minimum-distance spectrum of the original kernel of size 2

$$T_2 = \begin{pmatrix} 1 & 0 \\ 1 & 1 \end{pmatrix} \quad (9)$$

is straightforward: for dimension 1, the second row is used, achieving distance 2, while for dimension 2, both rows are used, achieving distance 1. Thus we have $S_{T_2} = (2, 1)$, with optimal row sets $\mathcal{R}_2^1 = \{1\}$ and $\mathcal{R}_2^2 = \{0, 1\}$; they are nested since $\mathcal{R}_2^1 \subset \mathcal{R}_2^2$. As a proof of concept for the different designs presented in Section IV, we introduce kernels

$$T_3 = \begin{pmatrix} 1 & 1 & 1 \\ 1 & 0 & 1 \\ 0 & 1 & 1 \end{pmatrix}, \quad T_5 = \begin{pmatrix} 1 & 1 & 1 & 1 & 1 \\ 1 & 0 & 0 & 0 & 0 \\ 1 & 0 & 0 & 1 & 0 \\ 1 & 1 & 1 & 0 & 0 \\ 0 & 0 & 1 & 1 & 1 \end{pmatrix} \quad (10)$$

for the construction of multi-kernel polar codes. We calculate their minimum-distance profiles and their decoding equations, showing their flexibility compared to kernels presented in [7].

The spectrum of T_3 can be calculated as follows. we select the first row (1 1 1) to maximize the minimum distance, giving minimum distance 3 and $\mathcal{R}_3^1 = \{0\}$; any other row selection would result in a smaller minimum distance, namely 2. For a code of dimension $K = 2$, the last two rows, (1 0 1) and (0 1 1), are selected, generating a code of minimum distance

2 with $\mathcal{R}_3^2 = \{1, 2\}$; any other row selection would result in a smaller minimum distance. Finally, the code of dimension $K = 3$ requires to select all rows having $\mathcal{R}_3^3 = \{0, 1, 2\}$, resulting in a code of minimum distance 1. The use of not-nested row sets like $\mathcal{R}_3^1 \not\subset \mathcal{R}_3^2$ allows for improved minimum-distance spectrum $S_{T_3} = (3, 2, 1)$ compared to [7] while keeping the same polarization rate $E = 0.42$.

A similar analysis for T_5 leads to the minimum-distance spectrum $S_{T_5} = (5, 3, 2, 1, 1)$ with optimal row sets $\mathcal{R}_5^1 = \{0\}$, $\mathcal{R}_5^2 = \{3, 4\}$, $\mathcal{R}_5^3 = \{2, 3, 4\}$, $\mathcal{R}_5^4 = \{1, 2, 3, 4\}$ and $\mathcal{R}_5^5 = \{0, 1, 2, 3, 4\}$. On the other side, its polarization rate is $E = 0.359$, which is worse than the rate of 0.431 achieved by optimal kernel in [7]. However, the optimal kernel has spectrum (4, 2, 2, 2, 1), limiting the achievable minimum distances of the full code to powers of 2; it is hard to state if proposed T_5 spectrum is better, since the full code distance depends on dimension and code length, however it permits a finer quantization in achievable minimum distances.

Decoding equations in reduced form can be calculated for the presented kernel; the ones for T_2 are the well known

$$\begin{aligned} f_0^2 : \lambda_0 &= L_0 \boxplus L_1, \\ f_1^2 : \lambda_1 &= (-1)^{\hat{u}_0} \cdot L_0 + L_1. \end{aligned}$$

The ones for T_3 given in (10) are

$$\begin{aligned} f_0^3 : \lambda_0 &= L_0 \boxplus L_1 \boxplus L_2, \\ f_1^3 : \lambda_1 &= (-1)^{\hat{u}_0} \cdot L_0 + L_1 \boxplus L_2, \\ f_2^3 : \lambda_2 &= (-1)^{\hat{u}_0} \cdot L_1 + (-1)^{\hat{u}_0 \oplus \hat{u}_1} \cdot L_2. \end{aligned}$$

Finally, the decoding equations for T_5 given in (10) are

$$\begin{aligned} f_0^5 : \lambda_0 &= L_1 \boxplus L_2 \boxplus L_4, \\ f_1^5 : \lambda_1 &= (-1)^{\hat{u}_0} \cdot (L_0 \boxplus L_3 \boxplus (L_2 + (L_1 \boxplus L_4))), \\ f_2^5 : \lambda_2 &= (-1)^{\hat{u}_1} \cdot (L_0 \boxplus L_1) + (L_3 \boxplus L_4), \\ f_3^5 : \lambda_3 &= (-1)^{\hat{u}_0 \oplus \hat{u}_1 \oplus \hat{u}_2} \cdot L_0 + (-1)^{\hat{u}_0} \cdot L_1 + (L_2 \boxplus (L_3 + L_4)), \\ f_4^5 : \lambda_4 &= (-1)^{\hat{u}_0 \oplus \hat{u}_3} \cdot L_2 + (-1)^{\hat{u}_0 \oplus \hat{u}_2} \cdot L_3 + (-1)^{\hat{u}_0} \cdot L_4. \end{aligned}$$

All expressions are optimal apart from f_2^5 . Conjecturing the original expression to be irreducible, we approximate it with a reducible one. This partially effects the decoding performance, however it allows for analytical determination of reliabilities to be used for code design as shown in Section IV-A.

IV. CODE DESIGN

Multi-kernel polar codes introduce new options in the code design, which for the original polar codes is limited to the selection of the information set according to reliabilites. In this section, we describe three design principles for multi-kernel polar codes, called the *reliability* design, the *distance* design and the *hybrid* design, theoretically motivating them and providing for each one a practical design algorithm.

A. Reliability Design

The reliability design is based on the polarization phenomenon and aims at minimizing the probability of error under SC decoding. This design is conceived for long codes, where channel polarization is strong enough to discriminate the channels properly. After a brief review of the concept, we will show how to determine these reliabilities, concluding the section with a discussion on the optimal kernels order.

We upper-bound the error probability under SC decoding of an (N, K) multi-kernel polar code with information set \mathcal{I} by

$$P_e^{\text{SC}} \leq \sum_{i \in \mathcal{I}} P_e(u_i), \quad (11)$$

where $P_e(u_i) = P(\hat{u}_i \neq u_i | \hat{u}_j = u_j, j < i)$ denotes the probability of making a wrong decision for bit \hat{u}_i assuming that all previously decoded bits are correct. The reliability design aims to minimize this upper bound so that the information set \mathcal{I}^R is chosen to contain the K most reliable positions. This is equivalent to finding the K positions minimizing the maximum error probability within these positions; \mathcal{I}^R can hence be found as the solution of the optimization problem

$$\begin{aligned} \min \quad & \max_{i \in \mathcal{I}} P_e(u_i) \\ \text{s.t.} \quad & \mathcal{I} \subset [N], |\mathcal{I}| = K. \end{aligned} \quad (12)$$

The simplest way to calculate the reliabilities is to use Monte-Carlo simulation, e.g. to run a genie-aided SC decoder to estimate the error rate of each input bit. In more detail, the all-zero codeword is transmitted over a channel with a target design SNR, and is decoded with a modified SC decoder that counts bit errors based on hard decisions of the LLRs but feeds back the correct decisions. As this method requires a large number of simulations to get stable results, we suggest to compute the approximated reliabilities of the input bits by density evolution under Gaussian approximation (DE/GA) [27] instead. If we suppose LLR distributions to be Gaussian, their variance is twice their mean value, i.e., $L_i \sim \mathcal{N}(m_i, 2m_i)$, permitting to follow their evolution by tracking their mean.

For DE/GA, the means are passed in the Tanner graph from the right to the left, similarly to LLRs. Looking at the Tanner graph block depicted in Fig. 2, we denote the mean of λ_i by μ_i , and the mean of L_j by m_j . For a BI-AWGN transmission system, the initial channel LLRs are distributed as $l_i \sim \mathcal{N}(\frac{2}{\sigma^2}, \frac{4}{\sigma^2})$, the initial mean value being $m_i = \frac{2}{\sigma^2}$ [28]. Under the Gaussian assumption, the error probability $P_e(u_i)$ is in direct correspondence with the LLR mean value μ_i as $P_e(u_i) = Q(\sqrt{\mu_i/2})$, where $Q(\cdot)$ denotes the tail probability of the standard Gaussian distribution; hence the SC error probability can be lower bounded by

$$P_e^{\text{SC}} \geq \max_{i \in \mathcal{I}} Q(\sqrt{\mu_i/2}). \quad (13)$$

To reduce the complexity of (12), error probabilities may be replaced LLR mean values; \mathcal{I}^R can then be determined solving

$$\begin{aligned} \max \quad & \min_{i \in \mathcal{I}} \mu_i \\ \text{s.t.} \quad & \mathcal{I} \subset [N], |\mathcal{I}| = K, \end{aligned} \quad (14)$$

where μ_i denotes the mean value of the LLR of u_i .

If kernel decoding equations (4) are expressed in reduced form, then the equations tracking the LLR means can be written directly: if LLRs L_0, \dots, L_{j-1} are independent, then

$$\mu(L_0 + \dots + L_{j-1}) = m_0 + \dots + m_{j-1} \quad (15)$$

$$\mu(L_0 \boxplus \dots \boxplus L_{j-1}) = \varphi_j(m_0, \dots, m_{j-1}), \quad (16)$$

where

$$\varphi_j(m_0, \dots, m_{j-1}) = \phi^{-1} \left(1 - \prod_{t=0}^{j-1} (1 - \phi(m_t)) \right), \quad (17)$$

$$\phi(m) = 1 - \frac{1}{\sqrt{4\pi m}} \int_{-\infty}^{+\infty} \tanh \frac{u}{2} e^{-\frac{(u-m)^2}{4m}} du. \quad (18)$$

We recall that functions ϕ and ϕ^{-1} can be approximated as

$$\phi(m) \approx \begin{cases} e^{am^2 - bm} & \text{if } 0 \leq m < c \\ e^{-\alpha m^\gamma + \beta} & \text{if } m \geq c \end{cases} \quad (19)$$

$$\phi^{-1}(m) \approx \begin{cases} \frac{b - \sqrt{b^2 + 4a \ln m}}{2a} & \text{if } 0 \leq m < c \\ \left(\frac{\beta - \ln m}{\alpha} \right)^{\frac{1}{\gamma}} & \text{if } m \geq c \end{cases} \quad (20)$$

Parameters $\alpha = 0.4527$, $\beta = 0.0218$, $\gamma = 0.86$, $a = 0.0564$, $b = 0.48560$, $c = 0.867861$ are acquired by curve-fitting [29].

The decoding equations for the kernels presented in Section II lead to the following evolution of mean values.

DE/GA for kernel T_2 :

$$\begin{aligned} \mu_0 &= \varphi_2(m_0, m_1) \\ \mu_1 &= m_0 + m_1 \end{aligned}$$

DE/GA for kernel T_3 :

$$\begin{aligned} \mu_0 &= \varphi_3(m_0, m_1, m_2) \\ \mu_1 &= m_0 + \varphi_2(m_1, m_2) \\ \mu_2 &= m_1 + m_2 \end{aligned}$$

DE/GA for kernel T_5 :

$$\begin{aligned} \mu_0 &= \varphi_3(m_1, m_2, m_4) \\ \mu_1 &= \varphi_3(m_0, m_3, (m_2 + \varphi_2(m_1, m_4))) \\ \mu_2 &= \varphi_2(m_0, m_1) + \varphi_2(m_4, m_4) \\ \mu_3 &= m_0 + m_1 + \varphi_2(m_2, m_3 + m_4) \\ \mu_4 &= m_2 + m_3 + m_4 \end{aligned}$$

The last point to be addressed is the selection of the order of kernels. The kernel order has two aspects. First, transformation matrices obtained by permuting the same kernels lead to equivalent codes by conveniently selecting the two information sets due to the permutation property of the Kronecker product. However, it is hard to predict the impact of the kernel order on the polarization of the input bits due to the non-linearity of function ϕ . Therefore codes of same length and dimension but different kernel orders may be different if reliability design is performed; as a result, for specific code dimensions, one kernel order may be preferable to others. We propose to perform an exhaustive search among all possible kernel orders to find the best one. For a code of dimension K , the metric used for the order selection is the sum of the reliabilities of the best K bits, and the kernel order giving the largest sum is retained.

B. Distance Design

In this section, we describe a design for multi-kernel polar codes maximizing the minimum distance of the resulting code [17]. This design is envisaged for short codes, where the polarization effect is not strong enough to prevail over the minimum distance properties. For an (N, K) multi-kernel polar code, the probability of error under maximum-likelihood (ML) decoding for the AWGN channel is bounded below as

$$P_e^{\text{ML}} \geq Q(\sqrt{d\mu/2}), \quad (21)$$

where d denotes the minimum distance of the code and $\mu = 2/\sigma^2$ the mean of the channel LLR. If the information set \mathcal{I}^{D} is selected to maximize $d\mu$, then (21) is minimized; since μ is fixed, this corresponds to solving the optimization problem

$$\begin{aligned} \max \quad & d_N(\mathcal{I}) \\ \text{s.t.} \quad & \mathcal{I} \subset [N], |\mathcal{I}| = K, \end{aligned} \quad (22)$$

where $d_N(\mathcal{I})$ denotes the minimum distance of the code defined by the rows of T_N indexed by \mathcal{I} . We solve this problem in two steps: first, we calculate the optimal minimum distance through the minimum distance spectrum of T_N , then we find the information set achieving that distance.

Algorithm 1 Information set for minimum distance

- 1: Initialize the sets $\mathcal{I} = \emptyset$ and $\mathcal{R}_p^0 = \emptyset$
 - 2: Load vector $s_N = (2, 1)^{\otimes n} \otimes S_{T_p}$
 - 3: Load optimal row sets $\mathcal{R}_p^1, \dots, \mathcal{R}_p^p$
 - 4: **for** $k = 1 \dots K$ **do**
 - 5: $l = \text{argmax}(s_N)$
 - 6: $c = (l \bmod p)$
 - 7: $q = \lfloor \frac{N-l-1}{p} \rfloor$
 - 8: $\mathcal{I} = (\mathcal{I} \setminus (\mathcal{R}_p^c + qp)) \cup (\mathcal{R}_p^{c+1} + qp)$
 - 9: $s_N(l) = 0$
 - 10: **end for**
 - 11: **return** \mathcal{I}
-

Though finding the minimum-distance spectrum of a code is in general a complex task, for polar codes it can be easily computed as $S_{T_2^{\otimes n}} = \text{sort}([2 \ 1]^{\otimes n})$, where the vector is sorted in descending order [30]. This property can be generalized to multi-kernel polar codes as follows.

Proposition 1. If $T_N = T_2^{\otimes n} \otimes T_p$, then

$$S_{T_N} = \text{sort}(S_{T_2^{\otimes n}} \otimes S_{T_p}) = \text{sort}([2 \ 1]^{\otimes n} \otimes S_{T_p}). \quad (23)$$

Proof: The property obviously holds for $n = 0$. By inductive hypothesis we now suppose that it holds for $n - 1$, i.e., that $S_{T_{N/2}} = \text{sort}(S_{T_2^{\otimes n-1}} \otimes S_{T_p})$. Defining $a^U = S_{T_{N/2}}$, $a^L = 2S_{T_{N/2}}$, such that $a = \text{sort}([a^U, a^L])$, the proposition is proved if $a = S_{T_N}$ since

$$\begin{aligned} \text{sort}(S_{T_{N/2}}, 2S_{T_{N/2}}) &= \text{sort}([2 \ 1] \otimes S_{T_{N/2}}) = \\ &= \text{sort}([2 \ 1] \otimes \text{sort}([1, 2] \otimes S_{T_{N/4}})) = \\ &= \text{sort}([2 \ 1] \otimes [1, 2] \otimes S_{T_{N/4}}) = \dots = \\ &= \text{sort}([2 \ 1]^{\otimes n} \otimes S_{T_p}). \end{aligned}$$

Consider a subcode of $T_N = \begin{pmatrix} T_{N/2} & 0 \\ T_{N/2} & T_{N/2} \end{pmatrix}$ defined by K rows, with K^U rows from $T^U = [T_{N/2} \ 0]$, K^L rows from $T^L = [T_{N/2} \ T_{N/2}]$, and $K^U + K^L = K$; denote the corresponding submatrices of T^U and T^L by T_A^U and T_B^L , respectively. If row indices are selected such that $d(T_A^U) = a^U(K^U)$ and $d(T_B^L) = a^L(K^L)$, which is possible by the induction hypotheses, then the minimum distance of this subcode is

$$\begin{aligned} d\left(\begin{bmatrix} T_A^U \\ T_B^L \end{bmatrix}\right) &\stackrel{(a)}{=} \min(d(T_A^U), d(T_B^L)) = \\ &= \min(a^U(K^U), a^L(K^L)) \stackrel{(b)}{=} a(K) \end{aligned}$$

where (a) follows from the distance property of the $(u|u+v)$ construction [31] and (b) from the sorting of two sorted lists. ■

Proposition 1 requires the transformation matrix of the code to be in the form $T_N = T_2^{\otimes n} \otimes T_p$. Note that this is not a limiting construction for the minimum-distance construction, since the minimum-distance spectrum does not depend on the order of the kernels in the Kronecker product. However, this structure permits to divide T_N into 2^n sub-matrices of p rows, termed as *sectors* in the following, each one consisting of a vector of T_p kernels and all-zero matrices. Analogously, information sets \mathcal{I} of size K can be split into 2^n smaller information sets $\mathcal{I}_q \subseteq [p]$, $|\mathcal{I}_q| = K_q \leq p$ and $\sum_q K_q = K$, where each \mathcal{I}_q collects the rows of the q -th sector included in \mathcal{I} . Since the minimum distance spectrum of q -th sector is given by $S_q = 2^{wt(q)} \cdot S_{T_p}$, where $wt(q)$ is the number of ones of q -th row of $T_2^{\otimes n}$, this division permits to identify the contribution of each sector to the minimum distance of the code. Due to the distance property of the $(u|u+v)$ construction, $d_N(\mathcal{I}) = \min(d_p(\mathcal{I}_1), \dots, d_p(\mathcal{I}_{2^n}))$; if \mathcal{I}_q is formed by the optimal row set $\mathcal{R}_p^{K_q}$, then $d_p(\mathcal{I}_q) = S_q(K_q)$.

This concept is exploited in greedy Algorithm 1 to design multi-kernel polar codes with optimal minimum distance. The algorithm adds sequentially row indices to the information set \mathcal{I} , modifying the information set of dimension $K-1$ to obtain the one for dimension K . Vector $s_N = [S_1 | \dots | S_{2^n}]$ formed by the minimum-distance spectra of the individual sectors is initially calculated as $s_N = (2, 1)^{\otimes n} \otimes S_{T_p}$; note that the vector is not sorted. At step k , the position l of the largest entry in s_N is extracted as $b = s_N(l)$, and $s_N(l)$ is set to zero. Then b represents the best minimum distance achievable by the code for dimension K ; q defined in line 7 identifies the sector to be updated to reach that distance; index $c = l \bmod p$ represents the number of rows of sector q already included in \mathcal{I} . To increase the value of c by one, the algorithm substitutes the previous optimal row set \mathcal{R}_p^c with the following one, i.e. \mathcal{R}_p^{c+1} , in line 8. The optimal row sets of the individual sectors need to be shifted by qp to be properly included in \mathcal{I} . The algorithm stops when \mathcal{I} comprises K elements.

Algorithm 1 requires the minimum-distance spectrum S_{T_p} and the optimal row sets of kernel T_p . A brute force calculation may be prohibitive for large kernels, since it is required to check the distances generated by all the $\binom{p}{k}$ possible k -rows sub-matrices of T_p . However, if $T_p = T_{p_1} \otimes T_{p_2}$, the kernel T_p can be divided into p_1 sectors of p_2 rows, each one formed

Algorithm 2 Spectrum of Kronecker product of kernels

```

1: Load optimal row sets  $\mathcal{R}_{p_1}^1, \dots, \mathcal{R}_{p_1}^{p_1}, \mathcal{R}_{p_2}^1, \dots, \mathcal{R}_{p_2}^{p_2}$ 
2: for  $k = 1 \dots p$  do
3:    $S_{T_p}(k) = 0$ 
4:    $\kappa = \text{ListPartition}(k, p_1, p_2)$ 
5:   for  $\ell = 1 \dots \text{length}(\kappa)$  do
6:      $\langle k_1, \dots, k_t \rangle = \kappa(\ell)$ 
7:      $\mathcal{R} = \bigcup_{j=1}^t (\mathcal{R}_{p_2}^{k_j} + \mathcal{R}_{p_1}^t(j) \cdot p_2)$ 
8:      $m = \text{MinDist}(T_p(\mathcal{R}, :))$ 
9:     if  $m > S_{T_p}(k)$  then
10:        $S_{T_p}(k) = m$ 
11:        $\mathcal{R}_p^k = \mathcal{R}$ 
12:     end if
13:   end for
14: end for
15: return  $\mathcal{R}_p^1, \dots, \mathcal{R}_p^p, S_{T_p}$ 

```

by the juxtaposition of kernels T_{p_2} . Then the set of k row indices, given by \mathcal{R}_p^k , is partitioned according to the sectors, indexed by the set $\{i_1, \dots, i_t\}$, and within each sector there are k_j rows, $j = 1, \dots, t$, where $k = \sum_{j=1}^t k_j$. Given this structure, we propose to limit the search space for the sector indices and for the index sets within the sectors to optimal row sets of the component kernels.

In more detail, an optimal row set $\mathcal{R}_{p_1}^t = \{i_1, \dots, i_t\}$ identifies the indices of the sectors that will contribute to \mathcal{R}_p^k ; for every retained sector i_j , an optimal row set $\mathcal{R}_{p_2}^{k_j}$ is included in \mathcal{R}_p^k . For each k , all the possible combinations of t and k_j have to be checked. Algorithm 2 performs this task, comparing the minimum distances of the row sets generated by all integer partitions of k of maximum length p_1 , i.e. the set of all possible ways of writing k as a sum of up to p_1 positive integers not larger than p_2 . The integer partition $\langle k_1, \dots, k_t \rangle$, where $k = \sum_{i=1}^t k_i$, unambiguously identifies row set

$$\mathcal{R}_{\langle k_1, \dots, k_t \rangle} = \bigcup_{j=1}^t (\mathcal{R}_{p_2}^{k_j} + i_j \cdot p_2), \quad (24)$$

where $\mathcal{R}_{p_1}^t = \{i_1, \dots, i_t\}$ with $i_1 < \dots < i_t$. In practice, t sectors are included in the row set, whose indices are listed in $\mathcal{R}_{p_1}^t$. The j -th sector contributes with k_j rows, that are chosen according to the optimal row set of kernel T_{p_2} .

As an example, we show the steps performed by Algorithm 2 to compute the optimal row set \mathcal{R}_9^4 for kernel

$$T_9 = T_3 \otimes T_3 = \left(\begin{array}{ccc|ccc|ccc} 1 & 1 & 1 & 1 & 1 & 1 & 1 & 1 & 1 \\ 1 & 0 & 1 & 1 & 0 & 1 & 1 & 0 & 1 \\ 0 & 1 & 1 & 0 & 1 & 1 & 0 & 1 & 1 \\ \hline 1 & 1 & 1 & 0 & 0 & 0 & 1 & 1 & 1 \\ 1 & 0 & 1 & 0 & 0 & 0 & 1 & 0 & 1 \\ 0 & 1 & 1 & 0 & 0 & 0 & 0 & 1 & 1 \\ \hline 0 & 0 & 0 & 1 & 1 & 1 & 1 & 1 & 1 \\ 0 & 0 & 0 & 1 & 0 & 1 & 1 & 0 & 1 \\ 0 & 0 & 0 & 0 & 1 & 1 & 0 & 1 & 1 \end{array} \right).$$

In this case, only 3 integer partitions of $k = 4$ respect the required properties, namely $\langle 1, 3 \rangle$, $\langle 2, 2 \rangle$ and $\langle 1, 1, 2 \rangle$. The

optimal row sets associated to $\langle 1, 3 \rangle$ is given by (24) as

$$\mathcal{R}_{\langle 1, 3 \rangle} = (\mathcal{R}_{p_2}^1 + 1 \cdot 3) \cup (\mathcal{R}_{p_2}^3 + 2 \cdot 3) = \{3, 6, 7, 8\} \quad (25)$$

with minimum distance $\text{MinDist}(T_9(\mathcal{R}_{\langle 1, 3 \rangle}, :)) = 2$; similarly, Algorithm 2 calculates $\mathcal{R}_{\langle 2, 2 \rangle} = \{4, 5, 7, 8\}$ with minimum distance 4 and $\mathcal{R}_{\langle 1, 1, 2 \rangle} = \{0, 3, 7, 8\}$ with minimum distance 3. Algorithm 2 selects $\mathcal{R}_9^4 = \mathcal{R}_{\langle 2, 2 \rangle} = \{4, 5, 7, 8\}$, with $S_{T_9}(4) = 4$. The complete minimum-distance spectrum of T_9 obtained by running Algorithm 2 for $k = 1, \dots, 9$ is $S_{T_9} = (9, 6, 4, 4, 3, 2, 2, 2, 1)$. Note that this spectrum is optimal, as we verified by an exhaustive search. In general the spectrum achieved by Algorithm 2 may be suboptimal.

C. Hybrid Design

The reliability design is conceived for SC decoding, and therefore suited for very long codes, where SC decoding becomes asymptotically optimal. The distance design, on the other hand, is assuming ML decoding, and thus is suited for short codes under SCL decoding, where moderate list lengths approximate ML decoding very well. The hybrid design combines reliability and distance as design criteria, and it is particularly effective to construct multi-kernel polar codes for medium code lengths under SCL decoding.

To introduce the hybrid design principle, we partition the transformation matrix (1) of a multi-kernel polar code as

$$T_N = T_{N_r} \otimes T_{N_d}, \quad (26)$$

with $T_{N_r} = T_{p_1} \otimes \dots \otimes T_{p_\psi}$ and $T_{N_d} = T_{p_{\psi+1}} \otimes \dots \otimes T_{p_s}$. The two matrices T_{N_r} and T_{N_d} can be treated as transformation matrices of smaller multi-kernel polar codes, of length $N_r = p_1 \cdot \dots \cdot p_\psi$ and $N_d = p_{\psi+1} \cdot \dots \cdot p_s$ respectively, with $N = N_r \cdot N_d$; corresponding Tanner graph is depicted in Fig. 3. The idea is to apply the distance design to the left part of the graph, consisting of T_{N_d} blocks, and the reliability design to the right part of the graph, consisting of T_{N_r} blocks; indices ‘d’ and ‘r’ stand for distance and reliability, respectively. This hybrid design comprises a parameter, ψ , that allows to trade distance vs. reliability. Reliability and distance designs can be seen as extreme cases with $\psi = s$ and $\psi = 0$ respectively.

Consider now the following decoding principle. The normal SC decoder proceeds until all right-messages are available at the input to the first T_{N_d} block. The block makes a local ML decision, i.e., it decides for the most likely codeword, and this decision is fed back into the SC decoding process. SC decoding proceeds until all right-messages are available at the input to the second T_{N_d} block, which makes a local ML decision and feeds the result back into the decoding process. This continues until the last T_{N_d} block has made its decision. Note that this decoding principle can be approximated by a plain SCL decoder, where larger values of ψ may require larger list sizes to reach ML decoding of left blocks.

Consider now the probability of error of the local ML decision at the i -th T_{N_d} block, denoted by $P_e(\mathbf{u}_i)$ for any $i = 0, 1, \dots, N_r - 1$, assuming all previous decisions being error-free. By SC decoding, all incoming messages have the same reliability; imposing Gaussian approximation on the message densities, we denote the mean of the incoming

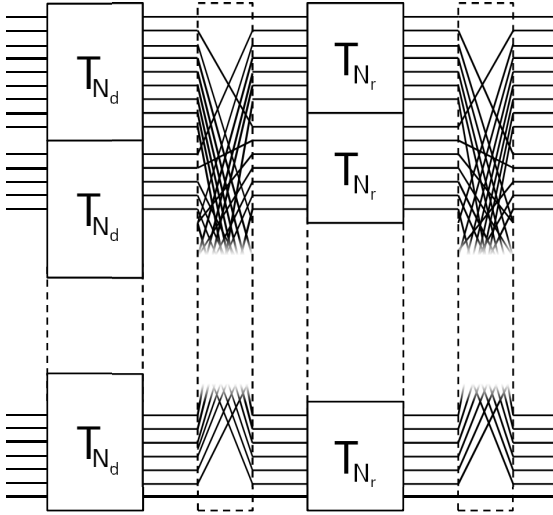


Fig. 3: Tanner graph of $T_N = T_{N_r} \otimes T_{N_d}$ for the hybrid design.

message density by μ_i and the minimum distance of the local code, as imposed by the information set on the T_{N_d} block, by d_i . The probability of error can thus be lower-bounded by

$$P_e(\mathbf{u}_i) \geq Q(\sqrt{d_i \mu_i / 2}), \quad (27)$$

while for the overall decoder is lower-bounded as

$$P_e^{\text{MLSC}} \geq \max_{i \in [N_r]} P_e(\mathbf{u}_i) \geq \max_{i \in [N_r]} Q(\sqrt{d_i \mu_i / 2}). \quad (28)$$

The information set \mathcal{I}^H of the hybrid design is selected to minimize this lower-bound, namely solving the optimization problem maximizing the minimum of the terms $d_i \mu_i$ as

$$\begin{aligned} \max \quad & \min_{i \in [N_r]} d_i(\mathcal{I}) \mu_i \\ \text{s.t.} \quad & \mathcal{I} \subset [N], |\mathcal{I}| = K, \end{aligned} \quad (29)$$

where $d_i(\mathcal{I})$ denotes the minimum distance of the code induced by \mathcal{I} over the i -th T_{N_d} block. This hybrid design minimizes the error rate for the mixed ML-SC decoder as described above. Note that both the bound (28) and the information set (29) are for a fixed value of $\psi \in [0, s]$, which may be adapted to the available list length of the SCL decoder.

The optimisation for the information set, as given in (29), can be solved slightly modifying Algorithm 1, introduced for the distance design in the previous section. Initially, the reliabilities of the N_r input bits of the partial transformation matrix T_{N_r} are determined using DE/GA, as described in Section IV-A. These reliabilities are stored in an intermediate vector $\mu = (\mu_{N_r-1}, \dots, \mu_0)$, where μ_i represents the reliability of the i -th input bit of the code generated by T_{N_r} . At the same time, the minimum distance spectrum of the partial transformation matrix T_{N_d} is computed, along with the optimal rows sets, using the methods for the distance design, as described in Section IV-B. Finally, vector $d_N = \mu \otimes S_{T_{N_d}}$, representing the "hybrid" spectrum of T_N , is calculated and given to Algorithm 1, along with the optimal rows sets calculated previously, to design the information set of the code.

D. Construction Example

We illustrate the proposed designs through a multi-kernel polar code of length $N = 12$ and dimension $K = 4$ with transformation matrix $T_{12} = T_2^{\otimes 2} \otimes T_3$ depicted in Fig. 1, i.e.

$$T_{12} = \begin{pmatrix} 1 & 1 & 1 & 0 & 0 & 0 & 0 & 0 & 0 & 0 & 0 & 0 \\ 1 & 0 & 1 & 0 & 0 & 0 & 0 & 0 & 0 & 0 & 0 & 0 \\ 0 & 1 & 1 & 0 & 0 & 0 & 0 & 0 & 0 & 0 & 0 & 0 \\ -1 & -1 & -1 & 1 & 1 & 1 & 0 & 0 & 0 & 0 & 0 & 0 \\ 1 & 0 & 1 & 1 & 0 & 1 & 0 & 0 & 0 & 0 & 0 & 0 \\ 0 & 1 & 1 & 0 & 1 & 1 & 0 & 0 & 0 & 0 & 0 & 0 \\ 1 & 1 & 1 & 0 & 0 & 0 & 1 & 1 & 1 & 0 & 0 & 0 \\ 1 & 0 & 1 & 0 & 0 & 0 & 1 & 0 & 1 & 0 & 0 & 0 \\ 0 & 1 & 1 & 0 & 0 & 0 & 0 & 1 & 1 & 0 & 0 & 0 \\ -1 & -1 & -1 & 1 & 1 & 1 & 1 & -1 & -1 & -1 & 1 & 1 & 1 \\ 1 & 0 & 1 & 1 & 0 & 1 & 1 & 0 & 1 & 1 & 0 & 1 & 1 \\ 0 & 1 & 1 & 0 & 1 & 1 & 0 & 1 & 1 & 0 & 1 & 1 & 1 \end{pmatrix},$$

for a BI-AWGN channel with inputs ± 1 and $\sigma^2 = 0.5$.

1) *Reliability design*: Using DE/GA, the reliabilities are calculated as (0.09, 1.28, 2, 1.85, 7.3, 9.12, 2.75, 9.57, 11.56, 11.94, 29.42, 32). The $K = 4$ most reliable positions form the information set: $\mathcal{I}^R = \{8, 9, 10, 11\}$.

2) *Distance design*: The minimum-distance spectrum and the optimal row sets of the kernel T_3 depicted in (10) are $S_{T_3} = (3, 2, 1)$ with $\mathcal{R}_3^1 = \{0\}$, $\mathcal{R}_3^2 = \{1, 2\}$ and $\mathcal{R}_3^3 = \{0, 1, 2\}$; the auxiliary vector is calculated as $d_{12} = (2, 1)^{\otimes 2} \otimes (3, 2, 1) = (12, 8, 4, 6, 4, 2, 6, 4, 2, 3, 2, 1)$. Algorithm 1 for $K = 4$ gives then $\mathcal{I}^D = \{3, 6, 10, 11\}$.

3) *Hybrid design*: Transformation matrix T_{12} includes $s = 3$ kernels, thus $\psi \in \{0, 1, 2, 3\}$. The hybrid design results in the reliability design for $\psi = 3$ and in the distance design for $\psi = 0$. For $\psi = 2$, we have $T_{N_r} = T_2^{\otimes 2}$ and $T_{N_d} = T_3$. The reliabilities of T_{N_r} are determined by DE/GA, resulting in $\mu = (16, 5.78, 4.56, 1)$, while S_{T_3} has been determined above. Thus we obtain the mixed spectrum $s_{12} = \mu \otimes S_{T_3} = (48, 32, 16, 17.34, 11.56, 5.78, 13.68, 9.12, 4.56, 3, 2, 1)$ for the transformation matrix T_{12} . This vector along with the optimal row sets for T_3 is used as input to Algorithm 1, giving the information set $\mathcal{I}^H = \{6, 9, 10, 11\}$ for $K = 4$. For $\psi = 1$ instead, we have $T_{N_r} = T_2$ and $T_{N_d} = T_2 \otimes T_3$, with vector $\mu = (8, 2.28)$. The minimum-distance spectrum of T_{N_d} can be calculated by Algorithm 2 as $S_{T_2 \otimes T_3} = (6, 4, 3, 2, 2, 1)$, with $\mathcal{R}_6^1 = \{3\}$, $\mathcal{R}_6^2 = \{4, 5\}$, $\mathcal{R}_6^3 = \{0, 4, 5\}$, $\mathcal{R}_6^4 = \{0, 3, 4, 5\}$, $\mathcal{R}_6^5 = \{1, 2, 3, 4, 5\}$ and $\mathcal{R}_6^6 = \{0, 1, 2, 3, 4, 5\}$. Algorithm 1 takes then as inputs $d_{12} = \mu \otimes S_{G_d} = (48, 32, 16, 24, 16, 8, 13.68, 9.12, 4.56, 6.84, 4.56, 2.28)$ and provides the information set $\mathcal{I}^H = \{6, 9, 10, 11\}$.

The four designs are summarized in Table I. As expected, distance design leads to the best minimum distance of 6, while the other designs yield a minimum distance of 4. In this case, $\psi = 1, 2$ result in the same information set, which is however different from the reliability design.

V. NUMERICAL EXAMPLES

In this section we evaluate the performance of the proposed multi-kernel polar codes under the different designs. All the simulations determine the BLock Error Rate (BLER) of the

ψ	\mathcal{I}	min. dist.
3 (rel.)	{8, 9, 10, 11}	4
2	{6, 9, 10, 11}	4
1	{6, 9, 10, 11}	4
0 (dist.)	{3, 6, 10, 11}	6

TABLE I: \mathcal{I} and minimum distances for (12, 4) codes.

codes for BI-AWGN channels under SCL decoding, usually for list size $L = 8$. To begin with, we evaluate the impact of the kernel order in the multi-kernel construction. Next, the impact of parameter ψ of the hybrid design is studied. Then we compare multi-kernel polar codes to punctured and shortened polar codes of same length and dimension. Finally, we compare multi-kernel polar codes with standard codes of same length and dimension, namely with LDPC codes for 802.11n [32] and polar codes for 5G NR [4].

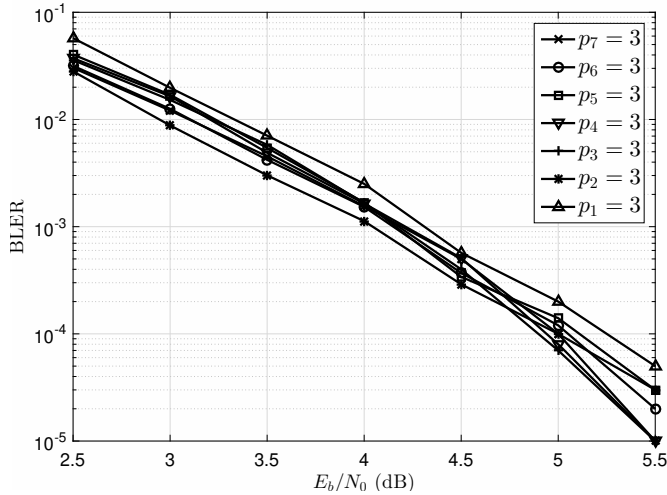


Fig. 4: BLER performance of (192, 96) multi-kernel polar codes under reliability design for different position of the unique T_3 kernel and list size $L = 8$.

Figure 4 shows the BLER performance of multi-kernel polar codes of length $N = 192 = 2^6 \cdot 3$ and rate $R = 1/2$, designed according to reliability, under SCL decoding with list size $L = 8$. The transformation matrix of this code is constructed mixing 6 kernels T_2 and a single T_3 kernel. There are hence 7 possible configurations of (1), namely depending on the position of the T_3 kernel in the Kronecker product. According to Figure 4, the performance gain between the best and the worst design for this code is about 0.5 dB. In particular, the best performance is obtained when $p_2 = 3$, i.e. when T_3 is placed in second position, while the worst performance is attained by switching the first two kernels of the best design, with $p_1 = 3$. Note also that the slope of the curves is different, which is due to differences in their distance properties. The metric proposed in Section IV-A for the selection of the kernel order suggests setting $p_3 = 3$, resulting in average performance at low SNR but quickly approaching the performance of $p_2 = 3$ at higher SNR.

Simulations confirm that the kernel order has some impact on the performance of multi-kernel polar codes under reliability design; no systematic behavior could be identified at this stage.

Figure 5 shows the BLER performance of multi-kernel polar codes of length $N = 384 = 2^7 \cdot 3$ and rate $R = 1/2$ under hybrid design for different values of parameter ψ introduced in Section IV-C. All the simulations are performed under SCL decoding with list size $L = 8$. In this case, the number of kernels composing the transformation matrix is $s = 8$, and the single T_3 kernel is placed in the last position, having $p_8 = 3$. Parameter ψ can hence span from 0 to 8, where the extreme cases $\psi = 0$ and $\psi = 8$ corresponding to distance and reliability designs, respectively, are highlighted with different colors. As expected for mid-length codes, distance design performs worse than reliability design, however the code is not long enough to have strong polarization. In this case, the mixed design offers an advantage over the other two designs due to higher flexibility. Simulations show that the performance strongly depends on the choice of parameter ψ ; a clear pattern is not recognizable and needs further studies. In the following, we set $\psi = \lceil \frac{s-1}{2} \rceil$ as a rule of thumb for the hybrid design.

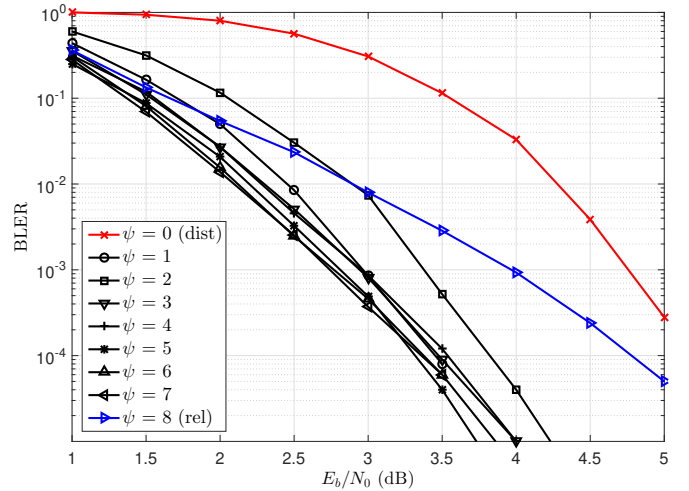


Fig. 5: BLER performance of (384, 192) multi-kernel polar codes under hybrid design for different values of ψ and $L = 8$.

Figure 6 shows a comparison between the presented multi-kernel polar codes under various designs and rate-matched polar codes for rate $R = 1/2$ under SCL decoding with $L = 8$. Polar codes of length N are generated from a mother polar code of length $M = 2^{\lceil \log_2(N) \rceil}$ through puncturing according to [10] and shortening according to [11]. The information sets of mother polar codes are hence calculated by either puncturing the first $M - N$ bits or shortening the last $M - N$ bits and calculating bit reliabilities through DE/GA [13]. Code lengths are selected to have a wide range of possibilities.

In Figure 6a the code length is set to $N = 144 = 3^2 \cdot 2^4$. This length can be reached by multi-kernel polar codes with two T_3 kernels and four T_2 kernels, while it demands strong puncturing/shortening by 144 bits to apply rate-matching from a mother polar code of length $M = 256$. Figure 6b shows the performance of codes of length $N = 200 = 5^2 \cdot 2^3$, reached by multi-kernel polar codes using two T_5 kernels in conjunction to

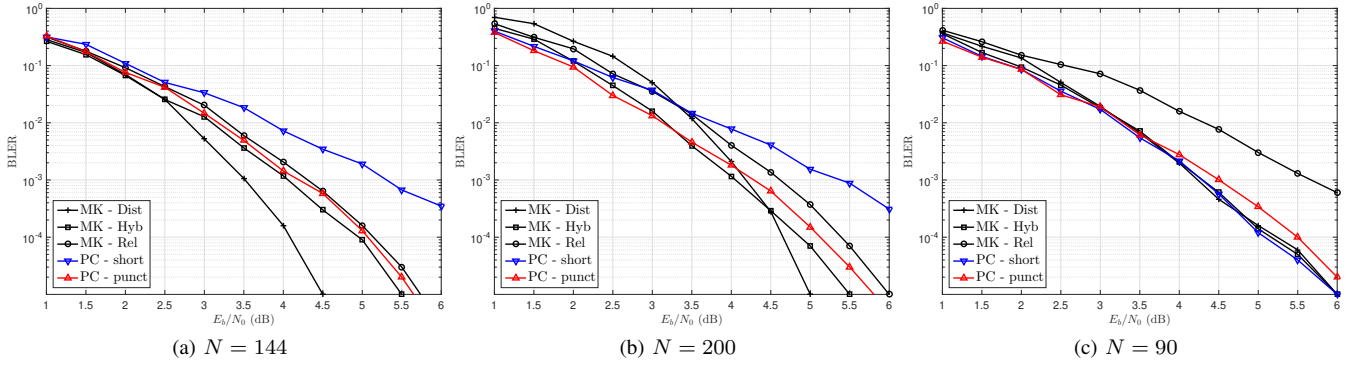


Fig. 6: BLER performance of multi-kernel polar codes compared with punctured [10] and shortened [11] polar codes of rate $R = 1/2$ under SCL decoding with $L = 8$.

T_2 kernels. The last Figure 6c mixes all the presented kernels showing the performance of codes of length $N = 90 = 5 \cdot 3^2 \cdot 2$.

Overall, we can see that reliability design of multi-kernel polar codes behaves similarly to the best rate-matching strategy among puncturing and shortening. The sub-optimality of T_5 LLR equation f_2^5 has an impact on the performance of the reliability design for short codes, as shown in Figure 6b. However, other designs are not impacted excessively by this issue, exhibiting good performance in this case. Moreover, distance design outperforms other designs for short codes, where minimum distance have still more impact than polarization effect; hybrid design permits a tradeoff between polarization and distance, always outperforming rate-matched polar codes.

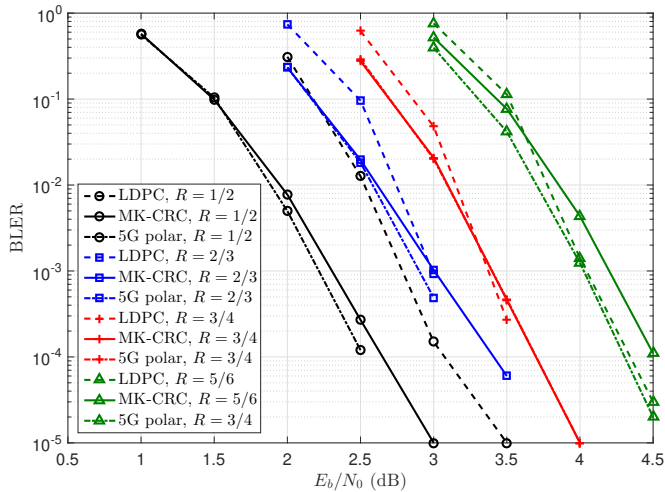


Fig. 7: BLER performance comparison among multi-kernel polar codes with 8 CRC bits, LDPC codes in [32] and polar codes standardized in 5G [4] for length $N = 1944$.

Figure 7 shows a comparison among multi-kernel polar codes, LDPC codes of the 802.11n standard [32] and polar codes standardized in 5G [4]. The 802.11n standard specifies the three code lengths 1944, 1296 and 648, and the four code rates $1/2$, $2/3$, $3/4$ and $5/6$; we show simulation results for $N = 1944$ and all four admissible rates. Multi-kernel polar codes are designed according to reliability, with the addition

of 10 CRC bits to help SCL decoding [2]. List size is set to $L = 8$ for both multi-kernel polar codes and 5G polar codes; LDPC codes are decoded using a 10-iterations offset min-sum decoder. Results show that the proposed multi-kernel polar codes are comparable to state-of-the-art channel codes.

VI. CONCLUSIONS

In this paper, we proposed a generalized polar code construction based on multiple kernels, termed multi-kernel polar codes. Though encoding and decoding resemble those of the original polar codes, as proposed by Arikan, multi-kernel polar codes provide various new design options. We presented such new code design principles based on reliability, distance, and a mix of those two as design criteria, coined as hybrid design, allowing to adapt the design to a given list length of the SCL decoder. The error-rate performance of multi-kernel polar codes was evaluated by simulations, resulting to be superior to state-of-the-art polar-code constructions, using puncturing or shortening methods, and state-of-the-art LDPC codes.

This paper focused on the information set design of multi-kernel polar codes. the design of optimal kernels or the optimization of hybrid design are not addressed in this paper and left for future research; the presented tools for analysis and design are believed to be useful for these purposes.

REFERENCES

- [1] E. Arikan, "Channel polarization: a method for constructing capacity-achieving codes for symmetric binary-input memoryless channels," *IEEE Transactions on Information Theory*, vol. 55, no. 7, pp. 3051–3073, July 2009.
- [2] I. Tal and A. Vardy, "List decoding of polar codes," in *IEEE International Symposium on Information Theory (ISIT)*, St. Petersburg, Russia, July 2011.
- [3] K. Niu and K. Chen, "CRC-aided decoding of polar codes," *IEEE Communications Letters*, vol. 16, no. 10, pp. 1668–1671, 2012.
- [4] V. Bioglio, C. Condo, and I. Land, "Design of polar codes in 5G New Radio," in *arXiv preprint arXiv:1804.04389*, April 2018.
- [5] S. B. Korada, E. Sasoglu, and R. Urbanke, "Polar codes: Characterization of exponent, bounds, and constructions," *IEEE Transactions on Information Theory*, vol. 56, no. 12, pp. 6253–6264, Dec. 2010.
- [6] N. Presman, O. Shapira, S. Litsyn, T. Etzion, and A. Vardy, "Binary polarization kernels from code decompositions," *IEEE Transactions on Information Theory*, vol. 61, no. 5, pp. 2227–2239, May 2015.

- [7] H.-P. Lin, S. Lin, and K. Abdel-Ghaffar, "Linear and nonlinear binary kernels of polar codes of small dimensions with maximum exponents," *IEEE Transactions on Information Theory*, vol. 61, no. 10, pp. 5253–5270, Oct. 2015.
- [8] R. Mori and T. Tanaka, "Non-binary polar codes using Reed-Solomon codes and algebraic geometry codes," in *IEEE Information Theory Workshop (ITW)*, Dublin, Ireland, September 2010.
- [9] N. Presman, O. Shapira, and S. Litsyn, "Mixed-kernels constructions of polar codes," *IEEE Journal on Selected Areas in Communications*, vol. 34, no. 2, pp. 239–253, 2016.
- [10] K. Niu, K. Chen, and J.-R. Lin, "Beyond turbo codes: Rate-compatible punctured polar codes," in *IEEE International Conference on Communications (ICC)*, Budapest, Hungary, June 2013.
- [11] R. Wang and R. Liu, "A novel puncturing scheme for polar codes," *IEEE Communications Letters*, vol. 18, no. 12, pp. 2081–2084, Dec. 2014.
- [12] L. Zhang, Z. Zhang, X. Wang, Q. Yu, and Y. Chen, "On the puncturing patterns for punctured polar codes," in *IEEE International Symposium on Information Theory (ISIT)*, Hawaii, U.S.A., July 2014.
- [13] V. Bioglio, F. Gabry, and I. Land, "Low-complexity puncturing and shortening of polar codes," in *IEEE Wireless Communications and Networking Conference (WCNC)*, San Francisco, USA, March 2017.
- [14] M. K. Lee and K. Yang, "The exponent of a polarizing matrix constructed from the kronecker product," *Designs, codes and cryptography*, vol. 70, no. 3, pp. 313–322, March 2014.
- [15] F. Gabry, V. Bioglio, I. Land, and J.-C. Belfiore, "Multi-kernel construction of polar codes," in *IEEE International Conference on Communications (ICC)*, Paris, France, May 2017.
- [16] M. Benammar, V. Bioglio, F. Gabry, and I. Land, "Multi-kernel polar codes: Proof of polarization and error exponents," in *IEEE Information Theory Workshop (ITW)*, Kaohsiung, Taiwan, Nov. 2017.
- [17] V. Bioglio, F. Gabry, I. Land, and J.-C. Belfiore, "Minimum-distance based construction of multi-kernel polar codes," in *IEEE Global Communications Conference (GLOBECOM)*, Singapore, Dec. 2017.
- [18] M. Mondelli, S. H. Hassani, and R. L. Urbanke, "From polar to Reed-Muller codes: a technique to improve the finite-length performance," *IEEE Transactions on Communications*, vol. 62, no. 9, pp. 3084–3091, 2014.
- [19] R. Mori and T. Tanaka, "Channel polarization on q-ary discrete memoryless channels by arbitrary kernels," in *IEEE International Symposium on Information Theory (ISIT)*, Austin, Texas, USA, June 2010.
- [20] D. S. Bernstein, *Matrix mathematics: Theory, facts, and formulas with application to linear systems theory*, Princeton University Press, 2005.
- [21] A. Alamdar-Yazdi and F. R. Kschischang, "A simplified successive-cancellation decoder for polar codes," *IEEE communications letters*, vol. 15, no. 12, pp. 1378–1380, 2011.
- [22] K. Niu and K. Chen, "Stack decoding of polar codes," *Electronics letters*, vol. 48, no. 12, pp. 695–697, 2012.
- [23] G. Bonik, S. Goreinov, and N. Zamarashkin, "Construction and analysis of polar and concatenated polar codes: practical approach," in *arXiv preprint*, arXiv:1207.4343, July 2012.
- [24] Z. Huang, S. Zhang, F. Zhang, C. Duanmu, and M. Chen, "On the successive cancellation decoding of polar codes with arbitrary binary linear kernels," in *arXiv preprint*, arXiv:1701.03264, Jan. 2017.
- [25] H. Griesser and V. R. Sidorenko, "A posteriori probability decoding of nonsystematically encoded block codes," *Problems of Information Transmission*, vol. 38, no. 3, pp. 182–193, Mar. 2002.
- [26] J. Hagenauer, E. Offer, and L. Papke, "Iterative decoding of binary block and convolutional codes," *IEEE Transactions on Information Theory*, vol. 42, no. 2, pp. 429–445, 1996.
- [27] R. Mori and T. Tanaka, "Performance of polar codes with the construction using density evolution," *IEEE Communications Letters*, vol. 13, no. 7, pp. 519–521, July 2009.
- [28] S. Y. Chung, T. J. Richardson, and R. L. Urbanke, "Analysis of sum-product decoding of low-density parity-check codes using a Gaussian approximation," *IEEE Transactions on Information Theory*, vol. 47, no. 2, pp. 657–670, 2001.
- [29] J. Ha, J. Kim, and S. W. McLaughlin, "Rate-compatible puncturing of low-density parity-check codes," *IEEE Transactions on Information Theory*, vol. 50, no. 11, pp. 2824–2836, 2004.
- [30] N. Hussami, S. B. Korada, and R. Urbanke, "Performance of polar codes for channel and source coding," in *IEEE International Symposium on Information Theory (ISIT)*, Seoul, Korea, June 2009.
- [31] F. J. MacWilliams and N. J. A. Sloane, *The theory of error-correcting codes*, vol. 16, Elsevier, 1977.
- [32] "IEEE standard for information technology - local and metropolitan area networks - specific requirements - part 11: Wireless LAN medium access control (MAC) and physical layer (PHY) specifications," Mar 2012.